PAPER

Universal time delay in the recollision impact ionization pathway of strong-field nonsequential double ionization

IOP Publishing Journal of Physics B: Atomic, Molecular and Optical Physics
J. Phys. B: At. Mol. Opt. Phys. **50** (2017) 225601 (8pp) https://doi.org/10.1088/1361-6455/aa9009

Universal time delay in the recollision impact ionization pathway of strong-field nonsequential double ionization

Qianguang Li[1], Yueming Zhou[2,4] and Peixiang Lu[2,3]

[1] School of Physics and Electronic-information Engineering, Hubei Engineering University, Xiaogan 432000, People's Republic of China
[2] School of Physics, Huazhong University of Science and Technology, Wuhan 430074, People's Republic of China
[3] Laboratory of Optical Information Technology, Wuhan Institute of Technology, Wuhan 430205, People's Republic of China

E-mail: zhouymhust@hust.edu.cn and lupeixiang@hust.edu.cn

Received 13 July 2017, revised 23 September 2017
Accepted for publication 29 September 2017
Published 30 October 2017

Abstract

With the semiclassical ensemble model, we investigated the correlated electron dynamics in the recollision impact ionization (RII) pathway of strong-field nonsequential double ionization (NSDI) at different laser wavelengths. Our results show that there is a remarkable time delay (about 400 attoseconds) between double ionization and recollision for a considerable part of the RII events. This type of event is responsible for the valley structure in the correlated electron momentum spectra along the laser polarization direction. More interestingly, our results show that this time delay is independent of the wavelength. This universal time delay is of crucial importance for the comprehensive understanding of the correlated electron dynamics in NSDI.

Keywords: nonsequential double ionization, correlated electron dynamics, recollision impact ionization

(Some figures may appear in colour only in the online journal)

1. Introduction

Nonsequential double ionization (NSDI) is a fundamental process among the various types of intense laser-atom/molecule interaction processes [1]. It has attracted increasing attention since the first observation of the knee structure in the doubly charged ionization yield curve of Xe [2]. The particular interest in NSDI is the highly correlated behavior of the ionized electron pairs [3]. During the past three decades, a great number of experimental and theoretical studies have been performed on NSDI [4–22] and the underlying electron dynamics has been well explored. Generally, the mechanism of NSDI can be understood by the rescattering picture [23, 24], where the outermost electron firstly tunnels through the distorted potential barrier formed by the atomic potential and the intense laser field, and then the freed electron is accelerated by the oscillating field and impelled back to recollide with the parent ion inelastically after the electric field changes sign, leading to the ionization of the second electron. More specifically, ionization of the second electron occurs through two different pathways [25]. When the energy of the recollision electron is lower than the ionization threshold of the second electron, the second electron is excited firstly by the recollision and then ionized by the laser field, referred to as the recollision-induced excitation with subsequent field ionization (RESI) pathway. Usually, recollision occurs at the zero-crossing of the electric field of the laser and the excited electron ionizes around the first maximum of the electric field after recollision. Consequently, there is a time delay of about $T/4$ (T is the cycle of the laser field) between double ionization and recollision. With the increasing of the recollision energy, double ionization can occur through the recollision impact ionization (RII) pathway, where the second electron ionizes directly after recollision. In

[4] Author to whom all correspondence should be addressed.

contrast to RESI, it is usually accepted that there is no time delay between double ionization and recollision. Numerous studies have been performed to reveal the details of the correlated electron dynamics in RII [26–28].

The microscopic electron dynamics in NSDI strongly depends on the wavelength of the laser pulses. Previous studies on NSDI were mainly focused on the near-infrared (NIR) region. Recently, owing to the great advances in ultrafast laser technology [29], greater attention has shifted towards strong-field ionization in the longer wavelengths, e.g., the mid-infrared (MIR) region [30]. It has been experimentally shown that the microscopic electron dynamics of NSDI in the MIR region is very different from that in the NIR region [31–35]. For example, in NSDI of Xe by the NIR laser pulses, the correlated electron momentum distribution (CEMD) is almost uniformly spread in four quadrants over a wide range of laser intensity [36], while in the MIR region the distribution is mainly located in the first and third quadrants and appears as a pronounced cross-like behavior [35]. For other noble gases and molecules, it has also been reported that the double-hump structures in the ion momentum spectra become much more obvious in the MIR region [31–33]. It was demonstrated that in the MIR region, the contribution of the RII pathway is greatly enhanced [33, 34], which is responsible for the wavelength-dependent results. Thus, the longer wavelength is more ideal to study the correlated electron dynamics in the RII process of strong-field NSDI. Recently, several theoretical studies have reported to have explored the electron dynamics in RII using MIR laser pulses [37, 38].

In this paper, we performed a more profound investigation of the electron dynamics in the RII pathway of strong-field NSDI. We systematically studied the correlated electron dynamics of NSDI over a wide range of laser wavelengths from the NIR to the MIR region with a 3D semiclassical ensemble model. Our results show that at a fixed ponderomotive energy U_p, the details of the CEMD change with the change in the wavelengths of the laser pulses. Specifically, the CEMD along the laser polarization direction exhibits an obvious valley structure on the main diagonal in the first and third quadrants at a laser pulse of 800 nm. This valley structure gradually becomes blurred as the wavelength increases. Back analyzing of the classical trajectories shows that there is a considerable part of the RII events where the second electron does not ionize immediately after recollision but has a 'dwell time' of about 400 attoseconds. This is responsible for the valley structure in the CEMDs. Moreover, this dwell time is universal for all of the wavelengths we studied. It decreases when scaled with the laser period, which results in the wavelength-dependent valley structure in the CEMDs.

2. Theoretical method

An accurate description of NSDI requires numerically solving the multielectron time-dependent Schrödinger equation in an intense laser field. However, the computational demand is too large [39, 40]. In recent years, the classical (semiclassical) methods have been well developed and widely used [12–16, 41–43]. Though some quantum effects, such as interference [18, 19], can not be captured, the classical methods have been proved to be reliable and effective tools in studying NSDI. The classical methods succeeded not only in reproducing the experimental results [28, 44] but also in predicting various phenomena [45, 46]. Moreover, classical methods have the advantage of back-tracing the classical trajectories, through which the underlying process can be intuitively presented [47]. Thus, in this paper, the 3D semiclassical ensemble model [15] is used to study the NSDI of Ar at different wavelengths. We only study NSDI at the near-infrared and mid-infrared regions. For the shorter wavelengths, it has been previously shown that NSDI exhibits the features of multiphoton processes [48] where the semiclassical mode breaks down.

In this semiclassical ensemble model, the ionization of the first electron from the bound state to the continuous state is treated by the tunneling ionization theory [49, 50]. The subsequent evolution of the ionized electron and the bound electron in the combined Coulomb potential and the laser fields is determined by the Newtonian equation of motion (atomic units are used throughout unless stated otherwise):

$$\frac{\mathrm{d}^2\mathbf{r}_i}{\mathrm{d}t^2} = -\nabla[V_{ne}(\mathbf{r}_i) + V_{ee}(\mathbf{r}_1, \mathbf{r}_2)] - \mathbf{E}(t), \tag{1}$$

where the subscript i is the label of the two electrons, and $\mathbf{r}_i$ represents the coordinate of the ith electron. $\mathbf{E}(t)$ is the laser field, which is linearly polarized along the $\hat{\mathbf{x}}$ axis. $V_{ne}(\mathbf{r}_i) = -2/\sqrt{\mathbf{r}_i^2 + a^2}$ and $V_{ee}(\mathbf{r}_1, \mathbf{r}_2) = 1/\sqrt{(\mathbf{r}_1 - \mathbf{r}_2)^2 + b^2}$ denote the ion–electron and electron–electron interactions, respectively. The soft parameters a and b are introduced to avoid the Coulomb singularity in the ion–electron and electron–electron interaction potentials. In the two-electron system, only the Coulomb singularity in the ion–electron interaction potential may occur and lead to autoionization, and should be shielded with an appropriate soft parameter. For Ar, a is generally set to 1.5 to avoid autoionization and b is set to 0.01 [12, 51].

The initial position of the first, i.e., the tunneling electron, is determined by the equation in parabolic coordinates [15]:

$$-\frac{1}{4\eta} - \frac{1}{8\eta^2} - \frac{\varepsilon\eta}{8} = \frac{I_{p1}}{4}. \tag{2}$$

Here, $I_{p1} = -0.58$ a.u. is the ionization potential of Ar [16]. In the quasistatic approximation, the above field parameter ε is equal to the laser field at the tunneling time $E(t_0)$ and the tunneling probability is evaluated by [49]

$$w(t_0) = \left(\frac{2(-2I_{p1})^{1/2}}{|\varepsilon|}\right)^{\frac{2}{\sqrt{-2I_{p1}}}-1} \exp\left(\frac{-2(-2I_{p1})^{3/2}}{3|\varepsilon|}\right). \tag{3}$$

The initial velocity of the first electron is set to be $v_{x0} = 0$, $v_{y0} = v_{\perp 0}\cos(\theta)$, $v_{z0} = v_{\perp 0}\sin(\theta)$, and has the distribution [50]

$$w(v_{\perp 0}) = \frac{(-2I_{p1})^{1/2} v_\perp}{\pi|\varepsilon|} \exp\left(-\frac{v_{\perp 0}^2(-2I_{p1})^{1/2}}{|\varepsilon|}\right). \tag{4}$$

Thus, the weight of each classical trajectory is evaluated by $w(t_0, v_{\perp 0}) = w(t_0)w(v_{\perp 0})$ [15].

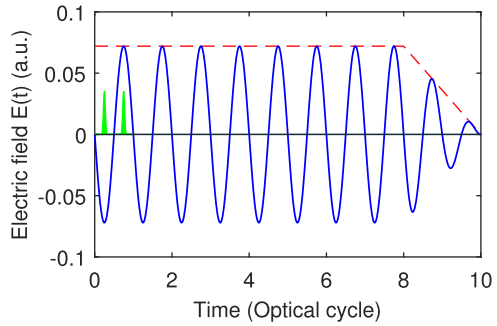

Figure 1. Electric field of the half trapezoidal laser pulse.

The initial state of the second, i.e., the bound electron, is determined by assuming that the electron is in the ground state of Ar $^+$, and described by a microcanical distribution. To obtain the initial values, the ensemble is populated starting from a classically allowed position. The available kinetic energy $E_k = I_{p2} + 2/\sqrt{\mathbf{r}^2 + a^2}$ is distributed randomly in momentum space. $I_{p2} = -1.01$ a.u. is the ionization potential of Ar $^+$ [16]. Then the electron is allowed to evolve a sufficiently long time (400 a.u.) in the absence of the laser field to obtain a stable position and momentum distribution.

After the laser field is turned off, we check the energies of both electrons at the end of the laser pulse, and a double ionization event is determined if both electrons achieve positive energies. Then we back trace the double ionization trajectories and find that all of the events experienced recollision and thus they are NSDI events. Several millions of weighted classical two-electron trajectories are traced from the tunneling moment to the end of the pulse, resulting in more than 10^4 NSDI events for our statistics.

3. Results and discussion

With this semiclassical model, we first calculated the NSDI of Ar by laser pulses at the fixed $U_p = 0.40$ a.u. with different wavelengths. Here the laser pulses have the half trapezoidal shape with a constant amplitude for the first eight cycles and a linear turning off at the last two cycles, as shown in figure 1. In these pulses, all of the NSDI events occur at the same laser intensity. In our calculations we only consider the NSDI events where tunneling of the first electron occurs during the first cycle of the laser field, as indicated by the green shading area in figure 1. Figure 2 presents the CEMDs along the laser polarization direction, where the laser wavelengths are (a) 800 nm, (b) 1200 nm, (c) 1600 nm and (d) 2000 nm, respectively. At first glance, the correlated electron spectra have roughly the same distributions, exhibiting prominent correlated behaviors, i.e., the electron pairs prefer to emit into the same hemisphere. Further inspection shows that there are visible differences among these spectra. At the shortest wavelength, the CEMD displays a clear valley structure on the main diagonal $p_{x1} = p_{x2}$ in the first and third quadrants, as shown in figure 2(a). When the laser wavelength increases, the distribution comes closer to the main diagonal, as shown in figure 2(b) for the 1200 nm pulse. The valley structure is

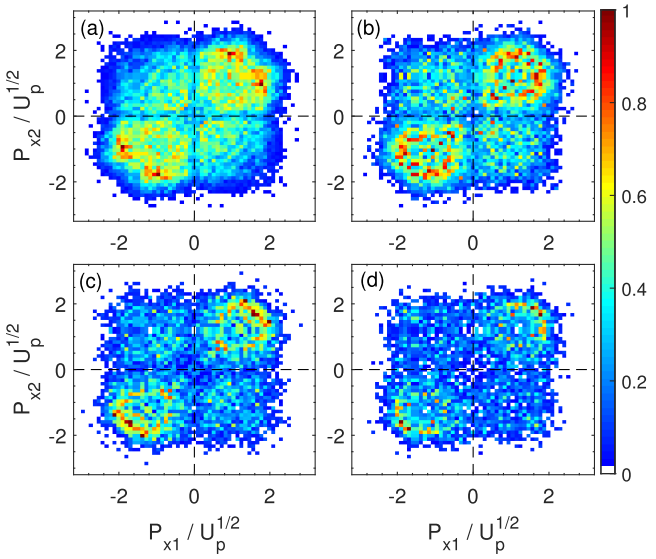

Figure 2. Correlated electron momentum distributions along the laser polarization direction for the NSDI of Ar by multicycle laser pulses with the ponderomotive potential $U_p = 0.40$ a.u. The wavelengths of the laser fields are (a) 800 nm, (b) 1200 nm, (c) 1600 nm and (d) 2000 nm.

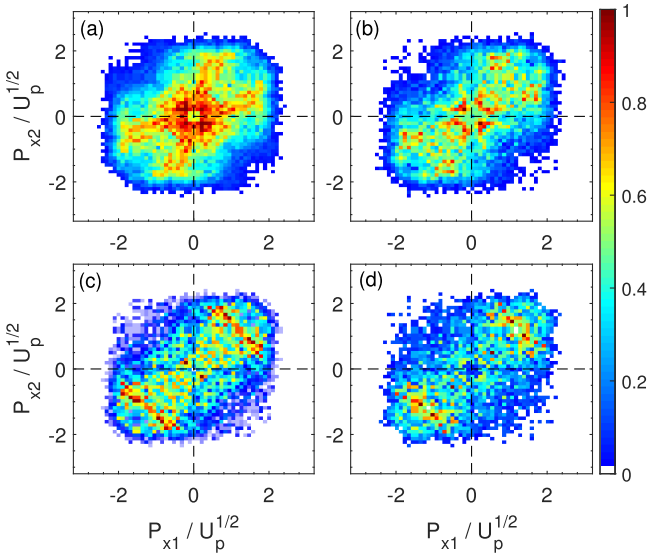

Figure 3. Correlated electron momentum distributions along the laser polarization direction for the NSDI of Ar by multicycle laser pulses with the ponderomotive potential $U_p = 0.69$ a.u. The wavelengths of the laser fields are (a) 800 nm, (b) 120 nm, (c) 1600 nm and (d) 2000 nm.

very faint at 1600 nm and almost disappears at 2000 nm, as shown in figures 2(c) and (d), respectively. This wavelength dependence phenomenon also occurs at a larger $U_p = 0.69$ a.u., as shown in figure 3.

In order to explore the origin of the wavelength dependence of the CEMD, we trace the NSDI classical trajectories and perform statistical analysis of the recollision and double ionization times. Here, the recollision time is defined as the instant of the closest approach of the two electrons after the tunneling of the first electron, and the double ionization time is defined as the instant when both electrons achieve

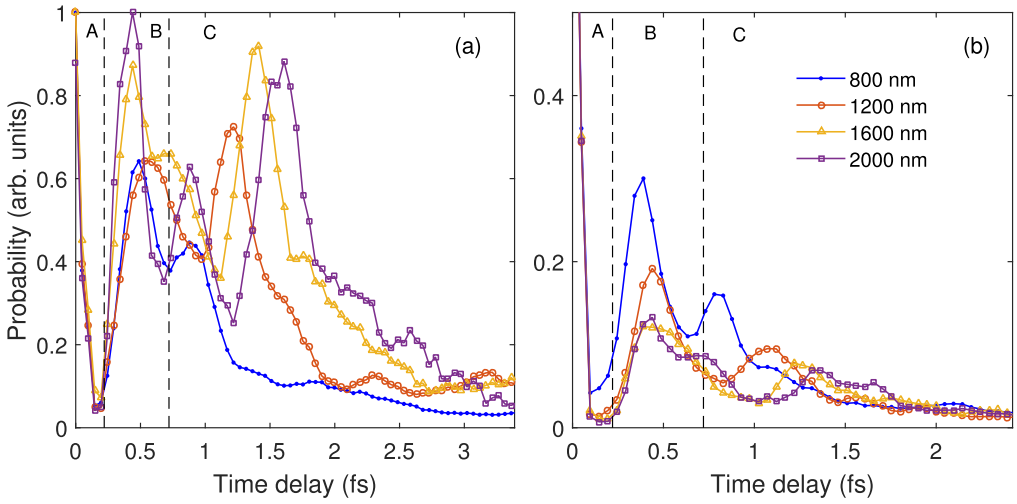

Figure 4. Time delay (t_d) between double ionization and recollision at 800 nm, 1200 nm, 1600 nm and 2000 nm. (a) and (b) correspond to the NSDI events in figures 1 and 2, respectively. Section A: $t_d < 0.24$ fs, section B: $0.24 < t_d < 0.72$ fs and section C: $t_d > 0.72$ fs. The data in each curve have been normalized so that the maximal value is one.

positive energies, where the energy of each electron contains the kinetic energy, potential energy of the electron–ion interaction and half of electron–electron repulsive energy. In figure 4 we show the time delay between the double ionization and the recollision. Surprisingly, for most of the NSDI events there is some time delay (t_d) between double ionization and recollision. In figure 4 we have divided the NSDI events into three sections according to the time delay, i.e., section A: $t_d < 0.24$ fs (10 a.u.), section B: $0.24 < t_d < 0.72$ fs, and section C: $t_d > 0.72$ fs (30 a.u.). In section A, the second electron ionizes immediately after recollision, which is the RII trajectories [25]. For section C, the peak of curve moves towards a larger time delay as the wavelength increases. Dividing this time delay by the laser cycle, we can find the peaks are located around $t_d = 0.2 \sim 0.3T$. This is the typical time delay in a RESI pathway [25]. The most interesting result is the peak around $t_d = 0.44$ fs in section B. It does not move with laser wavelength. This time delay is so short ($0.15T$ for the 800 nm field and $0.06T$ for the 2000 nm field) that the transient electric field at the ionization of the second electron is almost zero and thus this cluster of trajectories should be classified as RII events. For these RII events, the second electron does not ionize immediately after recollision, but dwells near the core for several hundreds of attoseconds and then gets ionized. For the case of the larger U_p, as shown in figure 4(b), this type of RII trajectories also exists and the dwell time almost does not change.

To explore the manifestation of these types of RII events in the experimentally accessible observations, we separately show the CEMDs according to the time delay between double ionization and recollision. The first, second and third rows in figure 5 display the CEMDs for the NSDI events with time delay $t_d < 0.24$ fs (panel A in figure 4(a)), $0.24 < t_d < 0.72$ fs (section B in figure 4(a)) and $t_d > 0.72$ fs (panel C in figure 4(a)), respectively. In the laser field with $U_p = 0.40$ a.u., the maximal energy ($3.17U_p$) of the recollision electron is larger than the ionization threshold of Ar^+, and consequently both the RII and RESI pathways occur in the NSDI processes. In the first and second rows, the NSDI events are well confined in the first and third quadrants in the CEMDs, showing the characteristics of RII [25]. In the third row, the CEMDs exhibit an almost uniform distribution in four quadrants, which is the typical distribution of the RESI pathway [25]. Close inspection shows that an obvious difference exists between the CEMDs in the first and second rows. In the first row, the distributions are clustered around the main diagonal, while in the second row the distributions exhibit a apparent minimum on the main diagonal. These valley structures can be understood as follows. In the first row the time delay between double ionization and recollision is approximately zero, i.e., the two electrons ionize almost simultaneously after recollision. To the first-order approximation [12], the electron's final momentum is determined by the ionization time. Thus, the two electrons achieve nearly the same final momentum for the NSDI events in the first row. For the laser parameters in our calculations, usually the energy of the first electron remains positive during the recollision process and thus the recollision time can be considered as the ionization time of the first electron after recollision. The time delay of about 0.44 fs in the second row makes the two electrons acquire different momenta from the laser field and results in the minima on the main diagonal in the first and third quadrants in the CEMDs. Moreover, when scaled with the laser period, this time delay decreases with the increasing of the laser wavelength. Thus the width of the valley becomes narrower as the wavelength increases. We note that the minimum on the main diagonal was observed in previous studies where it was referred to as finger-like shape [12, 52]. There, the finger-like shape comes from the NSDI events where the two electrons ionized simultaneously after recollision and the final-state electron–electron repulsion and electron–ion attraction were responsible. In our case, the two electrons escape one after the other, and thus the ionization time is responsible. Figure 6 shows the separated CEMDs for a higher recollision energy (with $U_p = 0.69$ a.u.). The distributions and the wavelength dependence show behaviors

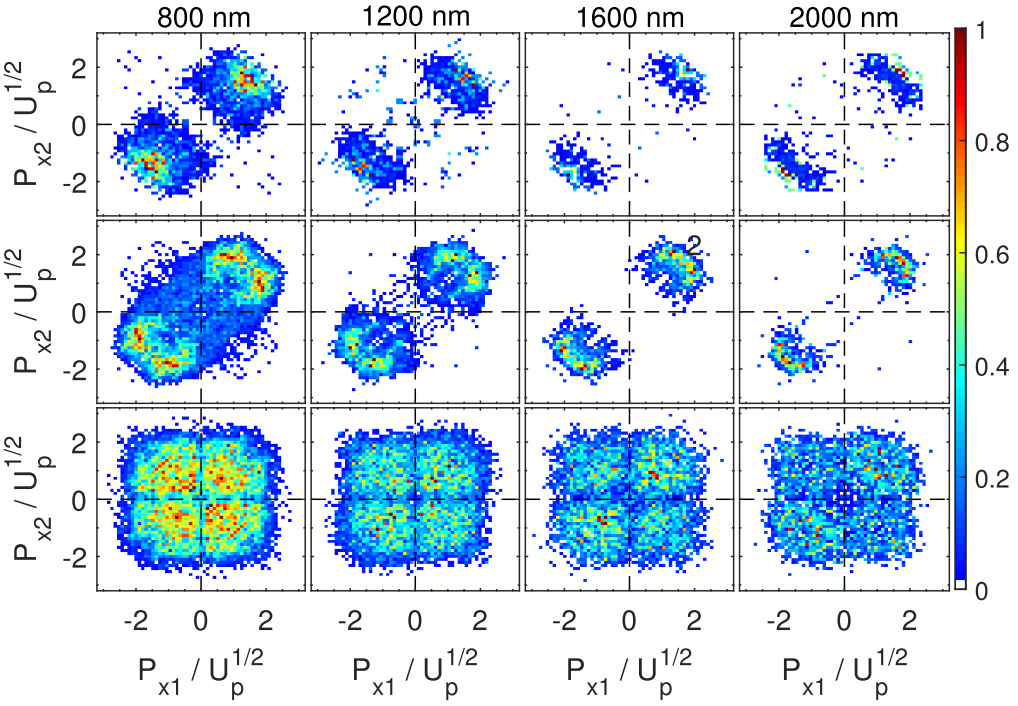

Figure 5. Correlated electron momentum distributions along the laser polarization direction for the NSDI in figure 1 with the time delay between the double ionization and recollision in the range of $t_d < 0.24$ fs (first row), $0.24 < t_d < 0.72$ fs (second row) and $t_d > 0.72$ fs (third row). The wavelengths of the laser fields from the first column to the fourth column are 800 nm, 1200 nm, 1600 nm, and 2000 nm, respectively.

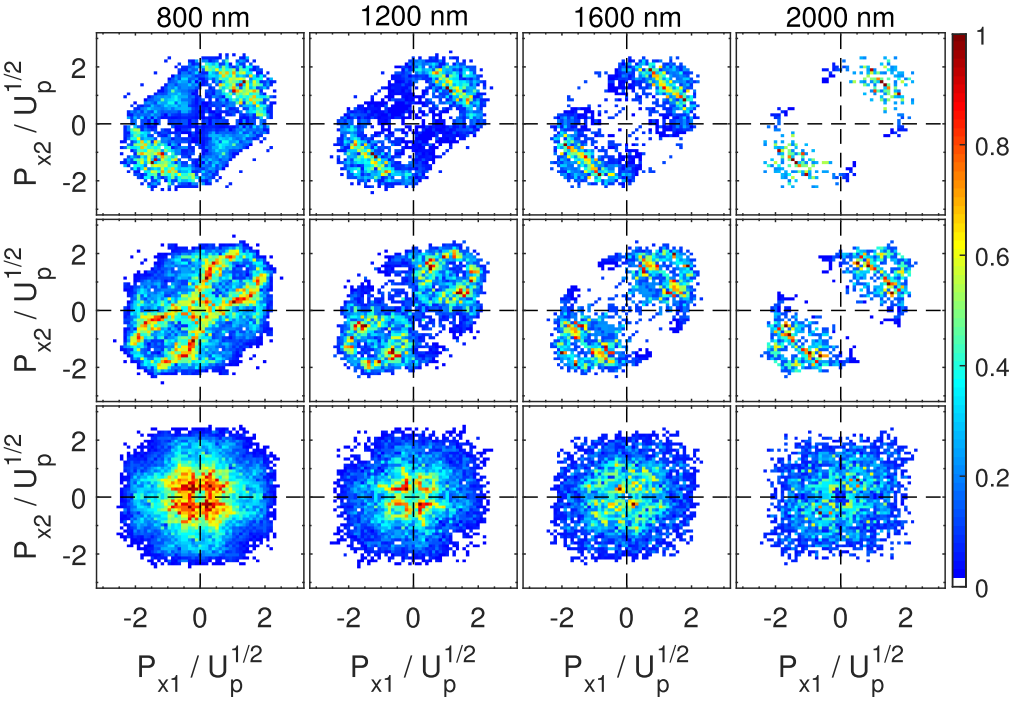

Figure 6. Correlated electron momentum distributions along the laser polarization direction for the NSDI events in figure 2 with the time delay between double ionization and recollision in the range $t_d < 0.24$ fs (first row), $0.24 < t_d < 0.72$ fs (second row) and $t_d > 0.72$ fs (third row). The wavelengths of the laser fields from the first column to the fourth column are 800 nm, 1200 m, 1600 nm and 2000 nm, respectively.

similar to those in figure 5. It should be noted that the type of RII events with a time delay of about 0.44 fs makes a considerable contribution to the total NSDI yields, as shown in figure 4. Figures 5 and 6 indicate that this type of NSDI process has a visible imprint in the experimental accessible observations. This type of NSDI event is responsible for the valley structure in the CEMDs in figures 2 and 3, and their wavelength-dependent details.

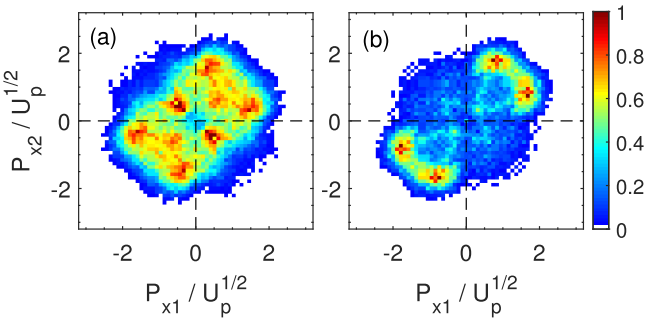

Figure 7. CEP-averaged correlated electron momentum distributions along the laser polarization direction for the NSDI of Ar by five-cycle laser pulses with the ponderomotive potential $U_p = 0.40$ a.u. The wavelengths of the laser fields are (a) 800 nm and (b) 2000 nm.

In the multicycle laser fields, the recollision repeats every half cycle, and there are many NSDI events where recollisions occur at the second and third returns [37, 38, 53]. The NSDI signals are the composite contribution of these trajectories. To see the RII pathway with a dwell time and its influence on the CEMD more definitely, we shift to NSDI by a few-cycle laser pulses, where the recollision process is much simpler [54, 55]. Figure 7 displays the CEMDs for the NSDI of Ar by five-cycle $\sin^2$-shaped laser pulses at $U_p = 0.40$ a.u. Here, the CEMDs are averaged over the carrier-envelope phases (CEP) from 0–2π, and the wavelengths of the laser pulses are 800 nm and 2000 nm in figures 7(a) and (b), respectively. It is clearly shown that both CEMDs exhibit obvious valley structures on the main diagonal in the first and third quadrants, and the width of the valley at 800 nm is broader than that at 2000 nm, which is similar to the results for the multicycle pulses shown in figures 2 and 3. To identify whether these phenomena are the results of the dwell time in the RII process, we traced the NSDI trajectories and in figure 8 we present the distributions of the time delay between the double ionization and recollision. Figures 8(a) and (b) display the CEP-resolved time delay for the cases of 800 nm and 2000 nm laser pulses, respectively. It is shown that there is also a very strong peak around 0.44 fs, and this peak does not change with CEP. Figure 8(c) shows the CEP-averaged distributions of the time delay for the 800 nm and 2000 nm fields. The peak around 0.44 fs hardly varies with the wavelength. It indicates that the RII pathway with a dwell time of several hundreds of attoseconds makes the dominant contribution to the NSDI, and the dwell time is universal.

Similar to figures 5 and 6, we separate the CEMDs in figure 7 into three parts according to the time delay. Figure 9 presents these separated CEMDs. In the first column ($t_d < 0.24$ fs), the CEMDs are almost the same for the 800 nm and 2000 nm fields, largely restrained in the first and third quadrants and clustered around the main diagonal. In the third column ($t_d > 0.72$ fs), where NSDI occurs through the RESI pathway, the distributions spread to the second and fourth quadrants. In the second column ($0.24 < t_d < 0.72$ fs), the electron pairs exhibit a clear minimum on the main diagonal in the first and third quadrants and the width of the valley at 2000 nm is much narrower than that at 800 nm, similar to the case of the multicycle laser fields. We mention again that this type of NSDI trajectory should be identified as the RII pathway because in the RESI pathway the second electron ionizes by the laser field at about $0.25T$ after recollision when the peak of the electric field of the laser arrives. Thus, the time delay in RESI depends on the laser wavelength. However, for the NSDI events we have shown here, the time delay is about 0.44 fs and is universal for all of the laser wavelengths we studied.

The microscopic electron dynamics of NSDI, including both the RII and RESI pathways, has been well explored in previous studies [56–58]. However, the time delay revealed in this paper has not been explored before. We note that in [57], a group of NSDI events with a time delay of about 0.15 laser cycle was observed for the NSDI by 800 nm laser pulses. There, this type of event was regarded as the RESI pathway because it was deemed that the second electron was ionized in assistance of the laser field after recollision. Identifying the role of the laser field in the ionization of the second electron is important. Our calculations show that this time delay does not change as the laser wavelength increases and thus it should be classified as the RII pathway, i.e., the laser field after recollision is not necessary for the ionization of the second electron. In a recent study [16], it was shown that at intensities well below the recollision threshold several optical cycles are required for the recolliding electron to thermalize the second electron through multiple recollisions. In our case, this time delay could probably be considered as the thermalization time. For the laser intensity near and above the recollision threshold, the thermalization takes about several hundreds of attoseconds.

4. Conclusion

In conclusion, we have systematically investigated the electron dynamics in the NSDI of Ar using a linearly polarized laser field with different wavelengths. We found that there is a dwell time of several hundreds of attoseconds for a considerable portion of the RII NSDI events. Moreover, this dwell time does not change with the laser intensity and wavelength. We have demonstrated that the dwell time has an obvious manifestation in the experimentally accessible correlated electron momentum spectrum. The wavelength dependence of the valley structure in the correlated electron spectra could be employed to indirectly confirm the electron dynamics revealed here.

In strong-field processes, the time information of ionization is of fundamental importance [59]. Considerable efforts have been made to identify the ionization time, particularly with the attoclcock technique [60]. For double ionization, knowledge of the ionization time of the two electrons after recollision is crucial to revealing the electron correlations. Recently, this time in the RESI pathway has been probed with the circularly polarized two-color pulses [61, 62]. Our results suggest a remarkable time delay for the ionization of the second electron in the RII pathway, in contrast to the previous

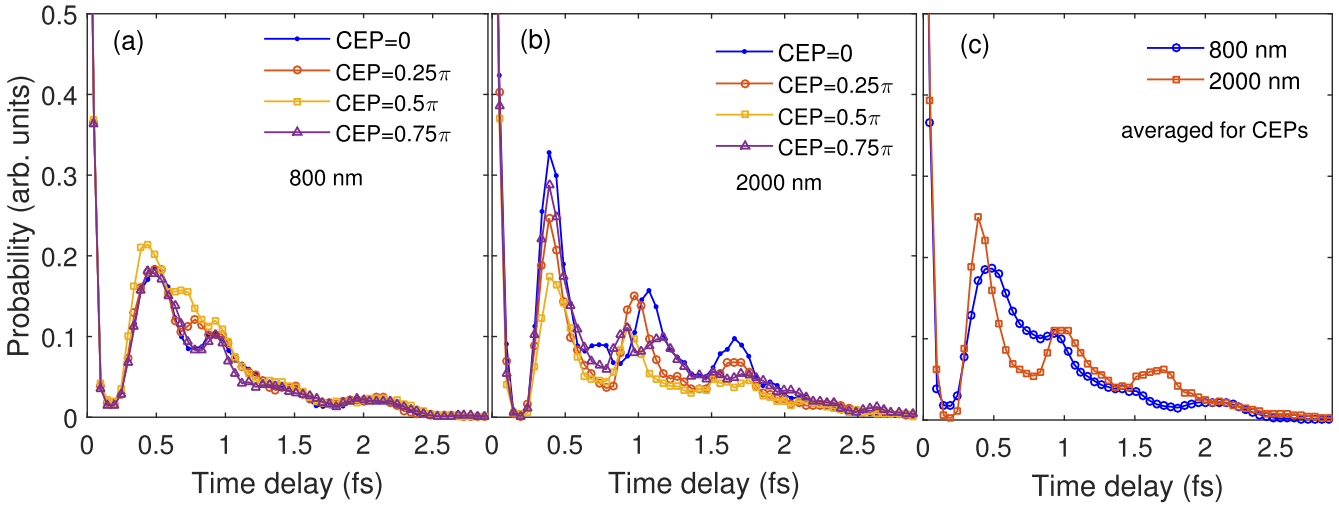

Figure 8. (a) and (b) CEP-resolved time delay between double ionization and recollision for the NSDI events in figures 6(a) and (b). Here four CEPs, i.e., 0, 0.25π, 0.5π and 0.75π, are presented. The wavelengths in (a) and (b) are 800 nm and 2000 nm, respectively. (c) CEP-averaged time delay between double ionization and recollision for the NSDI events in figures 6(a) and (b). The data in each curve have been normalized so that the maximal value is 1.

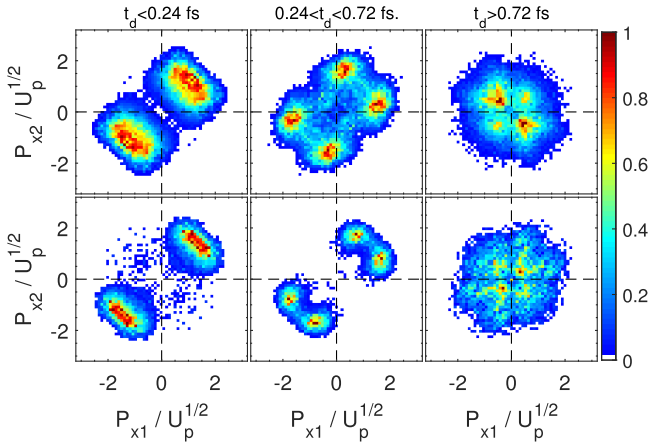

Figure 9. Correlated electron momentum distributions along the laser polarization direction for the NSDI in figure 6 with the time delay between the double ionization and recollision in the range of $t_d < 0.24$ fs (first column), $0.24 < t_d < 0.72$ fs (second column) and $t_d > 0.72$ fs (third column). The wavelengths of the laser fields of the first and second rows are 800 nm and 1200 nm, respectively.

understanding which supposes both electrons ionized immediately after recollision. The correlated behavior in the CEMDs is strongly affected by this time delay. Thus, it is important to consider this universal time delay for the comprehensive understanding of the correlated electron dynamics from the measured CEMDs.

Acknowledgments

This work was supported by the National Natural Science Foundation of China (NNSFC) (11622431, 11234004, 11547018) and the Natural Science Foundation of Hubei (NSFH) (2014CFB578).

ORCID iDs

Qianguang Li https://orcid.org/0000-0003-3090-3959

References

[1] Krausz F and Ivanov M 2009 *Rev. Mod. Phys.* **81** 163
[2] I'Huillier A, Lompre L A, Mainfray G and Manus C 1983 *Phys. Rev.* A **27** 2503
[3] Weber T, Giessen H, Weckenbrock M, Urbasch G, Staudte A, Spielberger L, Jagutzki O, Mergel V, Vollmer M and Dörner R 2000 *Nature (London)* **405** 658
[4] Fittinghoff D N, Bolton P R, Chang B and Kulander K C 1992 *Phys. Rev. Lett.* **69** 2642
[5] Chaloupka J L, Rudati J, Lafon R, Agostini P, Kulander K C and DiMauro L F 2003 *Phys. Rev. Lett.* **90** 033002
[6] Rudenko A, Zrost K, Feuerstein B, de Jesus V L B, Schröter C D, Moshammer R and Ullrich J 2004 *Phys. Rev. Lett.* **93** 253001
[7] Moshammer R *et al* 2000 *Phys. Rev. Lett.* **84** 447
[8] Becker A and Faisal F H M 2000 *Phys. Rev. Lett.* **84** 3546
[9] Weckenbrock M, Becker A, Staudte A, Kammer S, Smolarski M, Bhardwaj V R, Rayner D M, Villeneuve D M, Corkum P B and Dörner R 2003 *Phys. Rev. Lett.* **91** 123004
[10] Liu X, Figueira de Morisson Faria C, Becker W and Corkum P B 2006 *J. Phys.* B **39** L305
[11] Lu P, Zhang W, Gong X, Song Q, Lin K, Ji Q, Ma J, He F, Zeng H and Wu J 2017 *Phys. Rev.* A **95** 033404
[12] Haan S L, Van Dyke J S and Smith Z S 2008 *Phys. Rev. Lett.* **101** 113001
[13] Zhang Z, Bai L and Zhang J 2014 *Phys. Rev.* A **90** 023410
[14] Xu T, Ben S, Wang T, Zhang J, Guo J and Liu X 2015 *Phys. Rev.* A **92** 033405
[15] Fu L, Liu J, Chen J and Chen S 2001 *Phys. Rev.* A **63** 043416
[16] Ye D, Li M, Fu L, Liu J, Gong Q, Liu Y and Ullrich J 2015 *Phys. Rev. Lett.* **115** 123001
[17] Lein M, Gross E K U and Engel V 2000 *Phys. Rev. Lett.* **85** 4707
[18] Hao X, Chen J, Li W, Wang B, Wang X and Becker W 2014 *Phys. Rev. Lett.* **112** 073002

[19] Maxwell A S and Figueira de Morisson Faria C 2016 *Phys. Rev. Lett.* **116** 143001
[20] He M, Li Y, Zhou Y, Li M and Lu P 2016 *Phys. Rev.* A **93** 033406
[21] Wang Z, Li M, Zhou Y, Lan P and Lu P 2017 *Sci. Rep.* **7** 42585
[22] He M, Zhou Y, Li Y, Li M and Lu P 2017 *Opt. Quant. Electron.* **49** 232
[23] Schafer K J, Yang B, DiMauro L F and Kulander K C 1993 *Phys. Rev. Lett.* **70** 1599
[24] Corkum P B 1993 *Phys. Rev. Lett.* **71** 1994
[25] Feuerstein B *et al* 2001 *Phys. Rev. Lett.* **87** 043003
[26] Staudte A *et al* 2007 *Phys. Rev. Lett.* **99** 263002
[27] Rudenko A, de Jesus V L B, Ergler T, Zrost K, Feuerstein B, Schröter C D, Moshammer R and Ullrich J 2007 *Phys. Rev. Lett.* **99** 263003
[28] Zhou Y, Liao Q and Lu P 2010 *Phys. Rev.* A **82** 053402
[29] Rezvani S A, Hong Z, Pang X, Wu S, Zhang Q and Lu P 2017 *Opt. Lett.* **42** 3367
[30] Agostini P and DiMauro L F 2008 *Contemp. Phys.* **49** 179
[31] Alnaser A S, Comtois D, Hasan A T, Villeneuve D M, Kieffer J and Litvinyuk I V 2008 *J. Phys.* B **41** 031001
[32] Herrwerth O *et al* 2008 *New J. Phys.* **10** 025007
[33] DiChiara A D, Sistrunk E, Blaga C I, Szafruga U B, Agostini P and DiMauro L F 2012 *Phys. Rev. Lett.* **108** 033002
[34] Wang Y, Xu S, Quan W, Gong C, Lai X, Hu S, Liu M, Chen J and Liu X 2016 *Phys. Rev.* A **94** 053412
[35] Wolter B, Pullen M G, Baudisch M, Sclafani M, Hemmer M, Senftleben A, Schröter C D, Ullrich J, Moshammer R and Biegert J 2015 *Phys. Rev.* X **5** 021034
[36] Sun X *et al* 2014 *Phys. Rev. Lett.* **113** 103001
[37] Li Y, Wang X, Yu B, Tang Q, Wang G and Wan J 2016 *Sci. Rep.* **6** 37413
[38] Huang C, Zhong M and Wu Z 2016 *Opt. Express* **24** 28361
[39] Parker J S, Doherty B J S, Taylor K T, Schultz K D, Blaga C I and DiMauro L F 2006 *Phys. Rev. Lett.* **96** 133001
[40] Hu S 2013 *Phys. Rev. Lett.* **111** 123003
[41] Mauger F, Chandre C and Uzer T 2010 *Phys. Rev. Lett.* **105** 083002
[42] Huang C, Guo W, Zhou Y and Wu Z 2016 *Phys. Rev.* A **93** 013416
[43] Zhou Y, Li M, Li Y, Tong A, Li Q and Lu P 2017 *Opt. Express* **25** 8450
[44] Zhou Y, Huang C, Liao Q and Lu P 2012 *Phys. Rev. Lett.* **109** 053004
[45] Schöffler M S, Xie X, Wustelt P, Möller M, Roither S, Kartashov D, Sayler A M, Baltuska A, Paulus G G and Kitzler M 2016 *Phys. Rev.* A **93** 063421
[46] Zhang L *et al* 2014 *Phys. Rev. Lett.* **112** 193002
[47] Phay J H, Panfili R, Haan S L and Eberly J H 2005 *Phys. Rev. Lett.* **94** 093002
[48] Henrichs K *et al* 2013 *Phys. Rev. Lett.* **111** 113003
[49] Ammosov M V, Delone N B and Krainov V P 1986 *Zh. Eksp. Teor. Fiz.* **91** 2008
Ammosov M V, Delone N B and Krainov V P 1986 *Sov. Phys. JETP* **64** 1191
[50] Delone N B and Krainov V P 1991 *J. Opt. Soc. Am.* B **8** 1207
[51] Haan S L and Smith Z S 2007 *Phys. Rev.* A **76** 053412
[52] Ye D, Liu X and Liu J 2008 *Phys. Rev. Lett.* **101** 233003
[53] Ma X, Zhou Y and Lu P 2016 *Phys. Rev.* A **93** 013425
[54] Liu X *et al* 2004 *Phys. Rev. Lett.* **93** 263001
[55] Camus N *et al* 2012 *Phys. Rev. Lett.* **108** 073003
[56] Haan S L, Breen L, Karim A and Eberly J H 2006 *Phys. Rev. Lett.* **97** 103008
[57] Haan S L, Breen L, Karim A and Eberly J H 2007 *Opt. Express* **15** 767
[58] Emmanouilidou A, Parker J S, Moore L R and Taylor K T 2011 *New J. Phys.* **13** 043001
[59] Lan P *et al* 2017 *Phys. Rev. Lett.* **119** 033201
[60] Eckle P, Smolarskl M, Schlup P, Biegert J, Staudte A, Schöffler M, Muller H G, Dörner R and Keller U 2008 *Nat. Phys.* **4** 565
[61] Mancuso C A *et al* 2016 *Phys. Rev. Lett.* **117** 133201
[62] Eckart S *et al* 2016 *Phys. Rev. Lett.* **117** 133202